J Mater Sci (2019) 54:7438–7446

Ceramics

Cold sintering with dimethyl sulfoxide solutions for metal oxides

Xiaoyu Kang[1], Richard Floyd[1,*], Sarah Lowum[2], Daniel Long[1], Elizabeth Dickey[1], and Jon-Paul Maria[1,2]

[1] Department of Materials Science and Engineering, North Carolina State University, Raleigh, NC 27695, USA
[2] Department of Materials Science and Engineering, The Pennsylvania State University, University Park, PA 16802, USA

Received: 7 November 2018
Accepted: 4 February 2019
Published online: 13 February 2019

ABSTRACT

Cold sintering of ZnO and MnO with dimethyl sulfoxide (DMSO)-based solutions is demonstrated. For ZnO ceramics, density values approach 99% theoretical when cold-sintered at 180 °C with DMSO-HOAc and DMSO-$Zn(OAc)_2$ solutions. MnO densified with aqueous HOAc solutions produces ceramics of 84% theoretical density that contain significant amounts of $Mn(OH)_2$ secondary phases. In comparison, using DMSO-HOAc solutions produces density values of 94% theoretical at 250 °C with trace quantities of Mn_3O_4, verified via X-ray diffraction. Scanning electron microscope analysis of sample fracture surfaces containing Mn_3O_4 reveals numerous crystallites smaller than 100 nm that nucleate on or between the considerably larger starting MnO grains. With increasing temperature, these precipitates appear to coalesce and fill the porosity that remains after initial compaction. These results identify an avenue to cold sinter metal oxides that, in the presence of aqueous media, favor hydroxide formation which inhibits further densification.

Introduction

Low-temperature densification methods for ceramics have long been of interest. Densities greater than 90% at temperatures less than 400 °C have been demonstrated by both solvent-free approaches, such as field-assisted sintering techniques [1–3], and solvent-assisted approaches, such as cold sintering [4, 5]. This paper will focus on the cold sintering approach, which generally involves densification of ceramics below 300 °C in the presence of a transport phase (that is often an aqueous solution) under uniaxial pressure conditions [4, 5]. Cold sintering shares similarities to the hydrothermal hot pressing (HHP) method demonstrated by Yamasaki, et al. [6, 7] in the 1980s that uses a dynamically sealed autoclave and uniaxial pressing rods. More recent studies regarding HHP (although termed hydrothermal sintering) have noted similarities between the mechanisms of the two processes, but pointed out that cold sintering uses an open system and therefore any liquid phase present is transient, while HHP or hydrothermal sintering uses a closed system [8]. Cold-sintered ceramics with density values exceeding 90% theoretical are reported

Address correspondence to E-mail: rdfloyd@ncsu.edu

https://doi.org/10.1007/s10853-019-03410-1

from materials including alkaline molybdates, $NaNO_2$, KH_2PO_4, ZnO, V_2O_5, $BaTiO_3$, etc., though some require additional processing following cold sintering [9–15]. Several reports now show that ZnO, in particular, can be densified to 99% of its theoretical value under uniaxial loading in a conventional pellet die in the presence of either HOAc- or $Zn(OAc)_2$-containing solutions, as demonstrated by Funahashi et al. [14] and Kang et al. [16], respectively.

Studies to extend cold sintering to multiple material systems have identified aspects of formulations that make achieving high densities through this method challenging. These can be sorted into three main categories: (1) formulations with high tendency to form a hydroxide or hydrate phase at room temperature, (2) formulations with low solubility of the desired metal ion species in solution, and (3) formulations with slow mass exchange kinetics at the solid–liquid interface. In such cases, it can be difficult to avoid a final product that is either a non-porous composite or a porous single-phase green body [17].

The formulation aspect that appears particularly challenging is that in the presence of water, many binary oxides form hydroxides that are more stable than their oxides below several hundred degrees Celcius. These include the oxides of Group IA, IIA, and many other transition metals (i.e., MnO, Y_2O_3, Al_2O_3, CdO, etc.) [18]. Hydroxide formation is also a concern as it consumes water-based transport phases quickly, preventing dissolution–reprecipitation events that participate in densification. In this paper, we demonstrate the possibility to perform cold sintering using a non-aqueous-based liquid solution as a means to minimize hydroxide formation. The experiments are conducted in the ZnO and MnO systems with dimethyl sulfoxide (DMSO) as the liquid component of the transport phase. ZnO was chosen as it provides a model system for comparison with an aqueous-based solution, while MnO was chosen because it is a strong hydroxide former in the presence of water. Controlling secondary phase formation, such as hydroxides, is an important capability needed to advance cold sintering to a broader palette of materials systems.

Experiment details

Pure MnO (Sigma-Aldrich, 99% pure) and ZnO powders (Alfa Aesar, 99.9% pure) were ball-milled for 24 and 48 h, producing an average starting particle size of approximately 1–2 μm and 150 nm, respectively. A summary of solutions and their abbreviations used for experiments are shown in Table 1.

DMSO-based solutions were kept on a hot plate at 100 °C to remove residual moisture. The DMSO- or water-based solutions were added to the MnO or ZnO powder through a syringe and mixed with a SpeedMixer (FlackTek Inc.). The powder mixture was then poured in a half-inch diameter die with a 400 W band heater and pressed uniaxially with a hydraulic press under a pressure of 530 MPa for 30 to 60 min. Upon pressure application, the die was heated to a constant densification temperature that spanned 100 °C to 300 °C. After extraction from the die, the pellets were dried in an oven at 80 °C for a minimum of 12 h. Pellet density was determined by measuring sample mass and calculating sample volume from caliper dimensions. Relative density values were calculated using theoretical values of pure MnO (5.43 g/cm^3) and ZnO (5.61 g/cm^3). The crystalline phases were investigated with X-ray diffraction performed on the surface of the compacted pellets (XRD—Panalytical Empyrean, HighScore Plus with ICDD PDF-2 2010 database) and scanning transmission electron microscopy (STEM) with electron energy loss spectroscopy (EELS) (FEI Titan G2 80-300, 200 kV accel. voltage, with Gatan Enfina detector). Fracture surface morphology was investigated with field-emission scanning electron microscopy (FEI Verios 460L FESEM & Zeiss SIGMA VP-FESEM, 1 kV accel. voltage each).

Table 1 Liquid-phase solutions used for experiments in this paper and their corresponding abbreviations

Abbreviation	Solution
DAc	10 vol% HOAc + DMSO
DZnAc	0.67M $Zn(OAc)_2$ + DMSO
HAc	10 vol% HOAc + H_2O
HMnAc	1M $Mn(OAc)_2$ + 10 vol% HOAc + H_2O

Results and discussion

Details of ZnO densification by cold sintering using aqueous solutions are reported elsewhere [16]. As described in these reports, phase pure pellets with 99% of theoretical density can be achieved at a temperature of 120 °C with HOAc or $Zn(OAc)_2$ aqueous solutions. Compared to ZnO, MnO densification is more challenging due to hydroxide formation tendency. Figure 1 shows the tendency for secondary phase formation via X-ray diffraction patterns for MnO ceramic pellets cold-sintered using either water or HAc as the transport phase and a dwell temperature of 120 °C. Diffraction peaks from $Mn(OH)_2$ are present in both cases. The measured densities were 74% and 80%, respectively. With the HMnAc solution, X-ray peaks from hydroxide are reduced dramatically; however, a similar density of 80% was obtained. In spite of the low density, MnO pellets synthesized with all three solutions were mechanically robust. Fracture surfaces of MnO densified with these aqueous solutions are shown in Fig. 2.

For all three samples, considerable porosity can be observed. For MnO with pure water, grain surfaces are populated with crystallites that often feature a flake-like morphology which is consistent with the $Mn(OH)_2$ crystal habit [19]. Limited volume shrinkage was observed for these pellets, as expected, since water must be consumed for hydroxide formation. Such binding without volume shrinkage is similar to hydration in cold pressing of cements where new phases must form [20]. For MnO processed with aqueous HAc solutions, flattened grain junctions appear in the fracture surfaces, indicating some degree of densification by grain boundary formation. This potentially occurred in the starting period before liquid was consumed by hydroxide formation and when solution pH was low enough to have sufficient Mn^{2+} ions for mass transport. As with the case of pure water, populations of small particles are present at grain surfaces and intersections in MnO processed with HAc. These are likely a combination of $Mn(OH)_2$ and MnO that precipitate as water is consumed, pH increases, and Mn^{2+} becomes supersaturated in solution. Note, however, that plate-like crystals are less frequent and smaller, which is consistent with the X-ray data, i.e., broader, weaker hydroxide peaks. This result is consistent with the more acidic conditions in which hydroxide formation is less favorable [18].

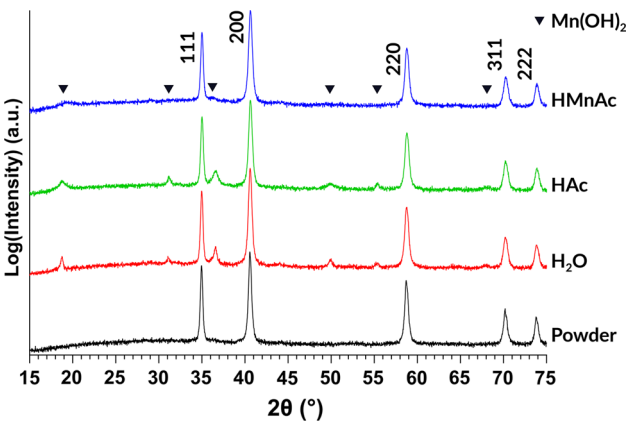

Figure 1 XRD of MnO starting powder and MnO pellets cold-sintered with water, HAc solution, and HMnAc solution. Experimental variables are 4 wt% liquid phase, 530 MPa, 120 °C, and 30-min process time. Reference codes are 01-075-0626 and 01-073-1604 for MnO and $Mn(OH)_2$, respectively.

MnO cold-sintered with HMnAc presents a different situation. X-ray diffraction in Fig. 1 shows only trace amounts of crystalline hydroxide. The SEM fracture surface in Fig. 2c shows much flatter grain surfaces with oriented geometric features that appear to be facets and few to no small particles in contrast to other solutions. Since the HMnAc solution contains additional Mn^{2+} ions from dissociation of the acetate, the concentration of Mn^{2+} will be greater compared to solutions where the ions come solely from the dissolution of MnO grain surfaces, thus favoring crystal nucleation. X-ray diffraction patterns show very little hydroxide phase, suggesting that precipitated material is primarily MnO. We cannot rule out some degree of precipitated manganese acetate or its decomposition product, but there is no evidence for this in the diffraction or SEM data [21]. Samples were prepared at higher temperatures using the same solutions. In all cases, though not shown in Fig. 1, hydroxide formation increased. The increasing fraction of $Mn(OH)_2$ is probably due to relatively slow heating rates compared to the rate of hydroxide formation; that is, the higher temperature promotes more rapid hydroxide formation well before the range it becomes unstable [19]. Furthermore, dehydration temperature tends to increase significantly with applied pressure [22]. Ultimately, when water is present and temperatures are increased, hydroxide formation seems unavoidable. In light of this result, the natural path forward is pursuing non-aqueous solutions. A candidate of choice is DMSO.

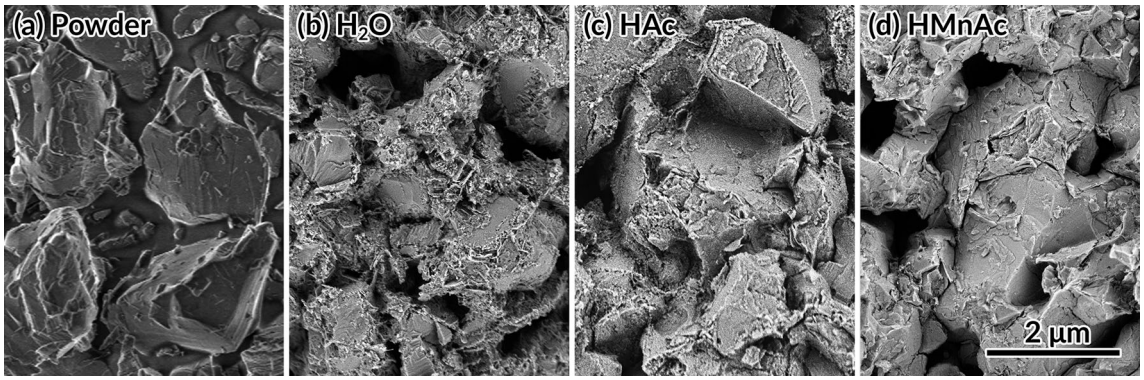

Figure 2 SEM of MnO **a** starting powder and pellets cold-sintered with **b** water, **c** HAc solution, and **d** HMnAc solution. Experimental variables are the same as Fig. 1.

As a reference, our initial experiment explores ZnO densification with DMSO instead of H_2O. DMSO has a high dielectric constant (47 at ambient conditions) contributing to similar solubility properties as water and can dissolve a significant amount of $Zn(OAc)_2$ (> 100 g per 100 ml) at room temperature. Ultimately DMSO-based solutions with similar concentrations of Zn^{2+} ions produced densification trends mirroring those observed with aqueous solutions when pressures, pressing times, and solution concentrations were the same. Density values above 99% theoretical were achieved with either DAc or DZnAc solutions. DMSO-based solutions require process temperatures between 180 and 200 °C, which is near the DMSO boiling point (189 °C), just as 120 °C (the preferred temperature for ZnO densification in aqueous liquid-phase systems) is near the $Zn(OAc)_2$ aqueous solution boiling point. We know that liquid additions must escape the sample for densification to occur [6, 15], and we speculate the temperatures near to the liquid-phase boiling points facilitate this escape by evaporation, promoting densification.

A typical microstructure of the ZnO starting powder and pellets densified with DAc solution is shown in Fig. 3. ZnO grains after cold sintering become equiaxed as compared to the starting powders with clean surfaces and very little pore space. Figure 4 shows XRD patterns of these ZnO pellets with only crystalline ZnO wurtzite peaks visible. These results are similar to aqueous solution-assisted densification results with the exception of more grain growth, which may be attributed to a higher process temperature [14].

MnO was used to investigate the applicability and potential secondary phase suppression of DMSO on densification of a known hydroxide former. Figure 5 shows a plot of final density of MnO as a function of pressing temperature at a constant pressure of 530 MPa, a 60-min dwell, and 5 wt% of DAc. The dashed blue line corresponds to mass loss during the post-densification drying step. Density increases with increasing temperature from 77% at 120 °C to 92% at 250 °C. At 120 °C, significant mass loss was observed after cold sintering, suggesting a large amount of residual transport phase. At temperatures above 180 °C, there is significant densification and much less residual solution, with a plateau at about 250 °C. Figure 6 shows X-ray diffraction data for this series. No $Mn(OH)_2$ diffraction peaks were observed in any sample; however, small reflections from Mn_3O_4 are present at all temperatures. The peak intensities do not depend strongly on process temperature. Mn_3O_4 may be generated from oxidation of dissolved Mn^{2+}, the MnO surfaces, or by the free radicals from DMSO decomposition [23, 24], discussed later. For reference, at ambient conditions, Mn_3O_4 is the more stable structure, so some conversion during cold sintering is expected [25].

SEM images of MnO fracture surfaces densified under varying temperatures are shown in Fig. 7. At a process temperature of 120 °C (Fig. 7a), the microstructure is porous, but porosity decreases significantly with increasing temperature. It is interesting to note the abrupt microstructural change at 180 °C, after which populations of small grains appear on the parent grain surfaces. This microstructural addition is a companion to a nearly 10% jump in density. With increasing temperature, porosity is reduced, and the population of small grains increases.

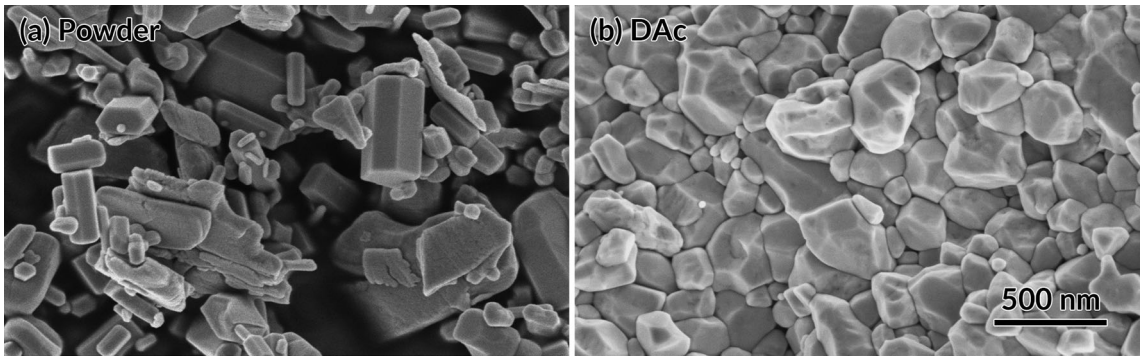

Figure 3 SEM of **a** powder and **b** fractured surface morphology of ZnO pellet densified with DAc solution at 180 °C and 530 MPa with 2 wt% liquid phase. The measured density was 98%.

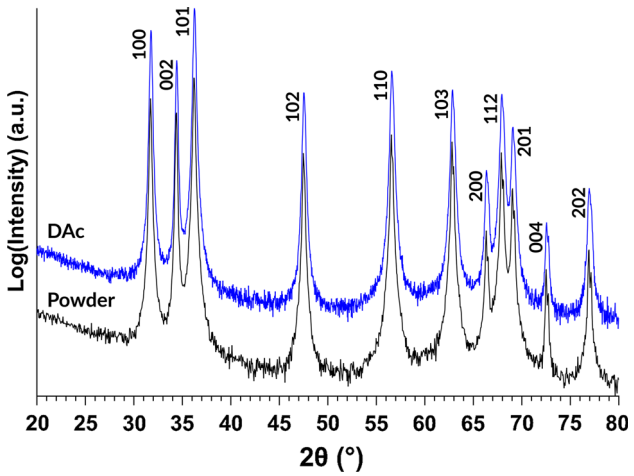

Figure 4 XRD of starting powder (black) and a ZnO pellet densified with DAc solution at 180 °C and 530 MPa with 2 wt% liquid phase (blue). Only crystalline wurtzite peaks are identifiable (reference code 00-036-1451).

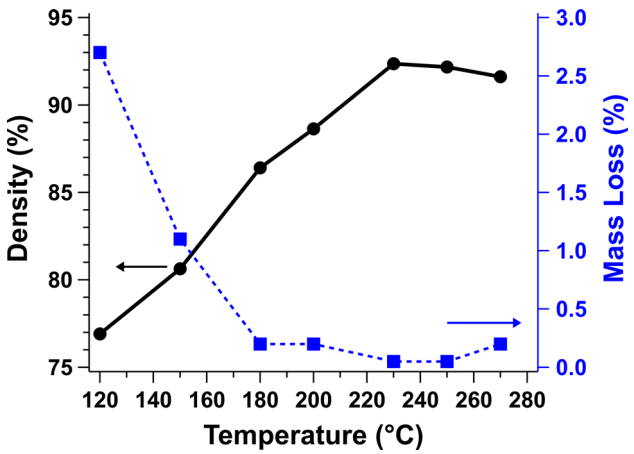

Figure 5 MnO pellets densified with DAc solution under varying temperatures. Pressure and process time were 530 MPa and 60 min, respectively. The blue dashed line represents mass loss after drying.

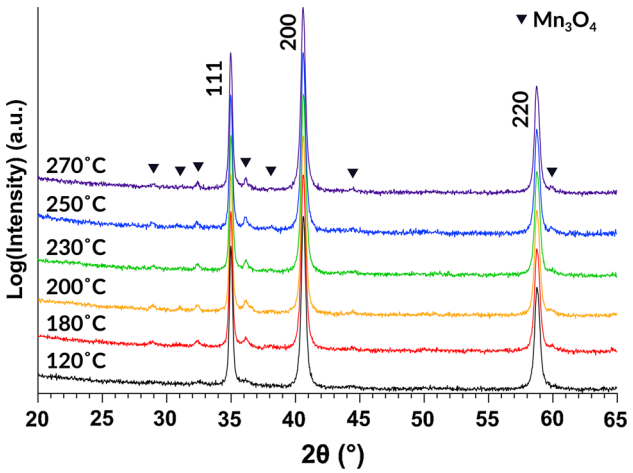

Figure 6 XRD of MnO pellets densified with varying process temperatures. Experimental conditions were 5 wt% of DAc, 530 MPa of pressure, and 60 min of process time. Reference codes are 01-075-0626 and 01-075-1560 for MnO and Mn_3O_4, respectively.

For MnO processed at 250 °C and 270 °C, there is a transition to larger grain diameters for newly formed grains. At first glance, this trend is difficult to understand as no additional Mn^{2+} ions are added by the transport phase. This means that the Mn^{2+} source for the newly forming grains must be the surfaces of the starting grains. Since the starting grains are much larger, their curvature should prevent dissolution and they should consume the smaller ones. However, the opposite trend occurs. The present data suggest a process where the applied uniaxial pressure causes stress concentrations at grain–grain contacts that can easily exceed 10 s of GPa at point contacts [5, 26, 27]. This in turn increases the local concentration of Mn^{2+} ions in solution that supports mass transport toward regions of lower concentration where precipitation

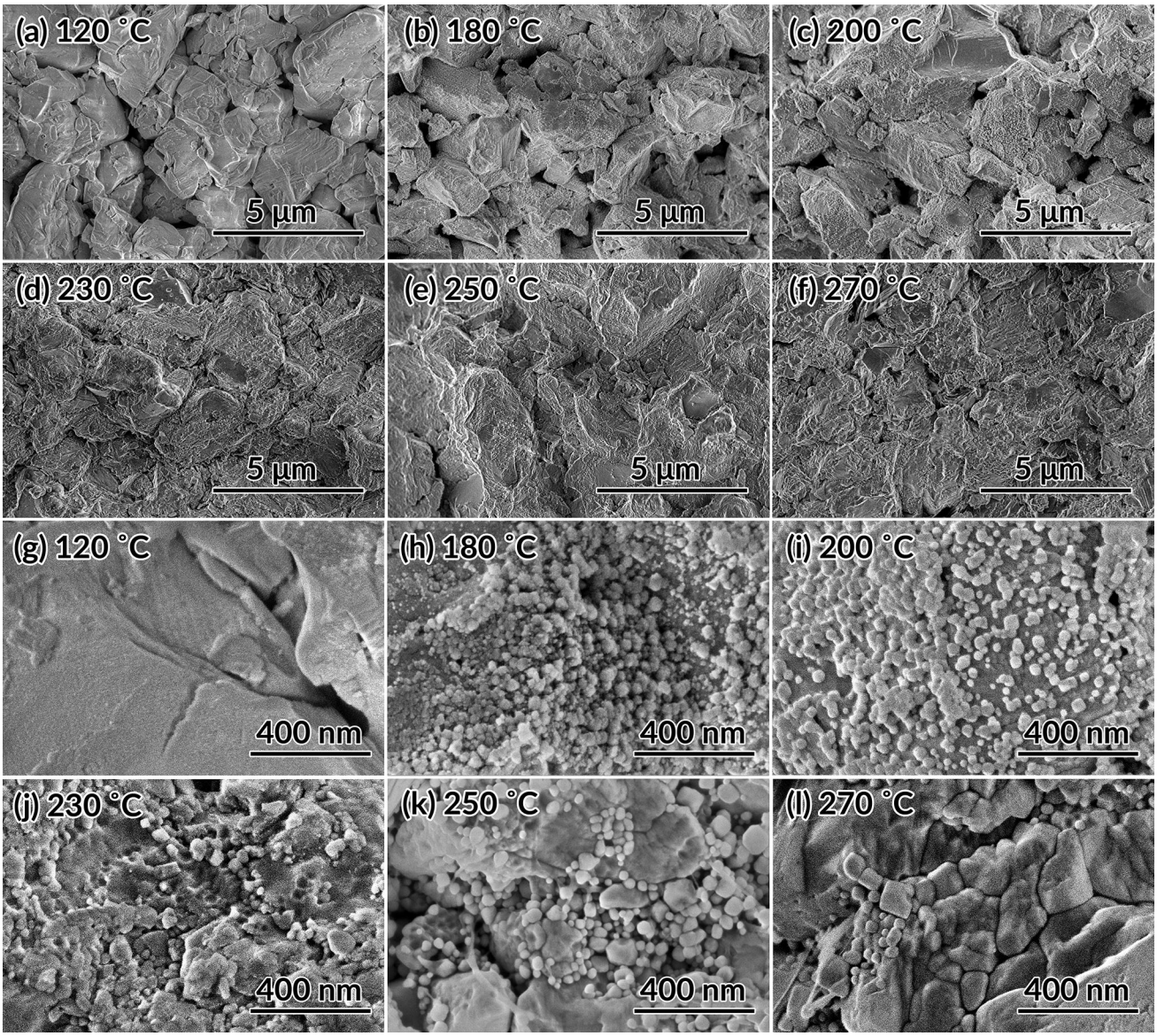

Figure 7 SEM images of fractured surfaces of MnO pellets densified with varying process temperatures: **a**, **g** 120 °C, **b**, **h** 180 °C, **c**, **i** 200 °C, **d**, **j** 230 °C, **e**, **k** 250 °C, and **f**, **l** 270 °C, with 5 wt% DAc solution, 530 MPa of pressure, and 60 min of process time.

and/or growth can occur. Increasing temperature increases the mass transport kinetics of this process, leading to the larger diameters of the precipitated grains. Unlike the aqueous analogue, competition from hydroxide formation is reduced, allowing densification to occur unfettered. Currently, the possibility of Mn^{3+} ions and/or DMSO decomposition playing a role in densification cannot be supported or refuted. As shown later, Mn^{3+} formation occurs during the densification process, but is limited to the surface of the parent and precipitate grains.

In summary, the collection of SEM images in Fig. 7 suggests a densification process driven by nucleation of small grains on the existing grain surfaces and within the interstitial volume of the parent grains. This produces a bimodal microstructure of grains roughly 50–200 nm in diameter (presumably precipitated new grains) superimposed among the original crystals with a grain size above 1 µm. As the cold sintering temperature increases, the size of the newly forming grains increases.

X-ray diffraction shows that trace amounts of Mn_3O_4 are present for all pellets pressed at temperatures above 120 °C. The relative intensity of Mn_3O_4 changed less than 2% at temperatures greater than 120 °C, while the average size of the small grain

population increased from ~ 25 to ~ 75 nm. Given the Mn_3O_4 peak and its negligible temperature dependence above 120 °C, we anticipate that only the surface of these small grains is composed of Mn_3O_4.

To be certain, STEM–EELS analysis was performed on a thinned MnO sample pressed at 250 °C. EELS signals of the oxygen K edge and the Mn $L_{2,3}$ edges were used to identify the Mn valence and to infer the crystal phase. Figure 8a shows a dark-field STEM image corresponding to a region with small grains (20–100 nm) at the boundary of a larger grain that is microns in diameter. Dots overlaid on this image correspond to locations where EELS spectra were collected. The locations were chosen such that sampling occurred over grain interiors, primarily for small grains that precipitated during the cold sintering process, and over grain boundaries. Spectra from each position are presented in Fig. 8b and referenced by color and number to their specific location. Spectra from grain interiors, which include a large parent grain and several smaller new grains, exhibit relatively sharp Mn $L_{2,3}$ edges, and spectra from the grain boundaries exhibit significant broadening and a ~ 1 eV shift of the Mn–$L_{2,3}$ edge. The broadening and shift to higher energy loss of the Mn L_3 peak in the grain boundary regions indicate the oxidation state of the interfaces is a mix of the bulk oxidation state and a higher oxidized Mn state [28]. With this result, we conclude that Mn_3O_4 is limited to the grain surfaces. Additional studies will determine when this apparent surface/grain boundary oxidation occurs.

Conclusions

In conclusion, cold sintering of ZnO and MnO with DMSO-based solutions is demonstrated. For ZnO, similar densification results as with aqueous solutions are obtained with DAc and DZnAc solutions: Over 99% of density is achieved with high phase purity. Densification of MnO was investigated with DAc solution with process temperatures from 120 to 270 °C. At 250 °C, maximum densities of 94% were achieved. In comparison, sintering in aqueous solutions could not exceed 80% at any temperature. Formation of $Mn(OH)_2$ is reduced significantly based on XRD phase identification. However, small amounts of Mn_3O_4 form, which is understood by the propensity for MnO to further oxidize even under ambient conditions. Small precipitates with dimensions between 50 and 200 nm nucleate and grow on the surface of MnO grains. EELS analysis of Mn valence suggests that these are MnO precipitates from the solution with Mn_3O_4 surface characteristics. Further improvement in MnO densification with DMSO-

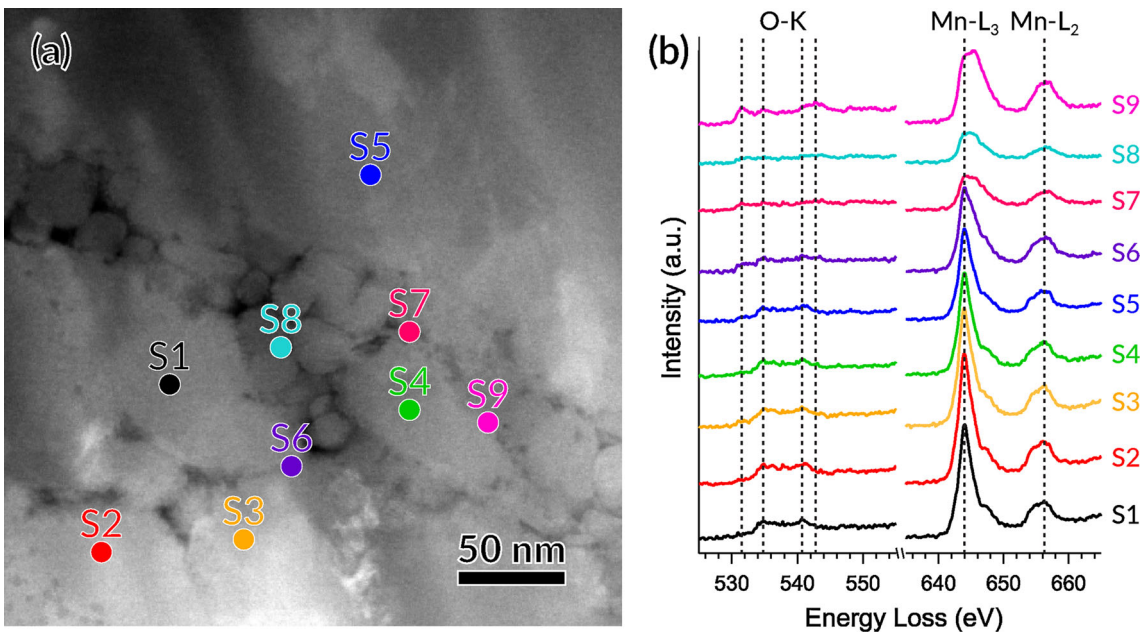

Figure 8 STEM image of precipitates at grain boundary (left) and EELS spectra (right) of O–K and Mn–L edges taken from location 1–10 for MnO cold-sintered with DAc solution at 250 °C, 530 MPa for 60 min.

based solutions should be possible with instrumentation designed to control die sealing and ambient gas environment in order to avoid contamination from atmospheric water. These results suggest that organic solvents with high polarities, such as DMSO, provide an interesting pathway to develop cold sintering process flows for an expanded number of oxide formulations.

Acknowledgements

This work was performed in part at the Analytical Instrumentation Facility (AIF) at North Carolina State University, which is supported by the State of North Carolina and the National Science Foundation (award number ECCS-1542015). The AIF is a member of the North Carolina Research Triangle Nanotechnology Network (RTNN), a site in the National Nanotechnology Coordinated Infrastructure (NNCI). The authors acknowledge support from The Center for Dielectrics and Piezoelectrics, a national research center and consortium under the auspices of the Industry/University Cooperative Research Centers program at the National Science Foundation under Grant Nos. IIP-1361571 and 1361503. The authors would like to acknowledge the use of the Huck Institutes of the Life Sciences' Microscopy and Cytometry Facility. This material is based upon work supported by the National Science Foundation Graduate Research Fellowship under Grant No. DGE-1746939. Any opinion, findings, and conclusions or recommendations expressed in this material are those of the authors(s) and do not necessarily reflect the views of the National Science Foundation.

Compliance with ethical standards

Conflict of interest The authors are unaware of any conflicts of interest regarding the data and findings presented in this manuscript.

References

[1] Herisson de Beauvoir T, Sangregorio A, Cornu I et al (2018) Cool-SPS: an opportunity for low temperature sintering of thermodynamically fragile materials. J Mater Chem C 6:2229–2233

[2] Dargatz B, Gonzalez-Julian J, Bram M et al (2016) FAST/SPS sintering of nanocrystalline zinc oxide-Part I: enhanced densification and formation of hydrogen-related defects in presence of adsorbed water. J Eur Ceram Soc 36:1207–1220

[3] Dargatz B, Gonzalez-Julian J, Bram M et al (2016) FAST/SPS sintering of nanocrystalline zinc oxide-Part II: abnormal grain growth, texture and grain anisotropy. J Eur Ceram Soc 36:1221–1232. https://doi.org/10.1016/j.jeurceramsoc.2015.12.008

[4] Maria JP, Kang X, Floyd RD et al (2017) Cold sintering: current status and prospects. J Mater Res 32:3205–3218

[5] Guo J, Floyd R, Lowum S et al (2019) Cold sintering: progress, challenges and future opportunities. Annu Rev Mater Res 49

[6] Yamasaki N, Yanagisawa K, Nishioka M, Kanahara S (1986) A hydrothermal hot-pressing method: apparatus and application. J Mater Sci Lett 5:355–356

[7] Yamasaki N, Weiping T, Jiajun K, Hosoi K (1995) Low-temperature sintering of calcium and magnesium carbonate by the hydrothermal hot-pressing technique. J Mater Sci Lett 14:1268–1270

[8] Goglio G, Ndayishimiye A, Largeteau A, Elissalde C (2019) View point on hydrothermal sintering: main features, today's recent advances and tomorrow's promises. Scr Mater 158:146–152

[9] Kähäri H, Teirikangas M, Juuti J, Jantunen H (2014) Dielectric properties of lithium molybdate ceramic fabricated at room temperature. J Am Ceram Soc 97:3378–3379

[10] Kähäri H, Teirikangas M, Juuti J, Jantunen H (2015) Improvements and modifications to room-temperature fabrication method for dielectric Li_2MoO_4 ceramics. J Am Ceram Soc 98:687–689

[11] Guo J, Guo H, Baker AL et al (2016) Cold sintering: a paradigm shift for processing and integration of ceramics. Angew Chem Int Ed 55:11457–11461

[12] Guo H, Baker A, Guo J, Randall CA (2016) Cold sintering process: a novel technique for low-temperature ceramic processing of ferroelectrics. J Am Ceram Soc 99:3489–3507

[13] Guo H, Baker A, Guo J, Randall CA (2016) Protocol for ultralow-temperature ceramic sintering: an integration of nanotechnology and the cold sintering process. ACS Nano 10:10606–10614

[14] Funahashi S, Guo J, Guo H et al (2017) Demonstration of the cold sintering process study for the densification and grain growth of ZnO ceramics. J Am Ceram Soc 100:546–553

[15] Guo H, Guo J, Baker A, Randall CA (2016) Hydrothermal-assisted cold sintering process: a new guidance for low-temperature ceramic sintering. ACS Appl Mater Interfaces 8:20909–20915

[16] Kang X, Floyd R, Lowum S et al (2019) Mechanism studies of hydrothermal cold sintering of zinc oxide at near room

temperature. J Am Ceram Soc. https://doi.org/10.1111/jace.16340
[17] Kang X (2017) Hydrothermal cold sintering. Thesis. North Carolina State University Repository
[18] Pourbaix M (1966) Atlas of electrochemical equilibria in aqueous solution, 1st edn. Pergamon Press, Oxford
[19] Oswald HR, Asper R (1977) Bivalent metal hydroxides. In: Lieth RMA (ed) Preparation and crystal growth of materials with layered structures. D. Reidel Publishing Company, Dordrecht, pp 71–140
[20] Roy DM (1987) New strong cement materials: chemically bonded ceramics. Am Assoc Adv Sci 235:651–658
[21] Mohamed MA, Halawy SA (1994) Kinetic and mechanistic study of the non-isothermal decomposition of manganese(II) acetate tetrahydrate. Thermochim Acta 242:173–186
[22] Kanzaki M (1991) Dehydration of brucite ($Mg(OH)_2$) at high pressures detected by differential thermal analysis. Geophys Res Lett 18:2189–2192
[23] Blank DA, North SW, Stranges D et al (1997) Unraveling the dissociation of dimethyl sulfoxide following absorption at 193 nm. J Chem Phys 106:539–550
[24] Head DL, McCarty CG (1973) The thermal decomposition of DMSO. Tetrahedron Lett 16:1405–1408
[25] Hem JD (1963) Chemical equilibria and rates of manganese oxidation. United States Department of the Interior, Washington, DC
[26] Kingery WD, Woulbroun JM, Charvat FR (1963) Effects of applied pressure on densification during sintering in the presence of a liquid phase. J Am Ceram Soc 46:391–395
[27] Coble RL (1970) Diffusion models for hot pressing with surface energy and pressure effects as driving forces. J Appl Phys 41:4798–4807
[28] Martens WN, Frost RL, Kristof J, Theo Kloprogge J (2002) Raman spectroscopy of dimethyl sulphoxide and deuterated dimethyl sulphoxide at 298 and 77 K. J Raman Spectrosc 33:84–91